# Supporting Information

## The adsorption characteristics and mechanism of C1 molecules on two-dimensional $SrTiO_3$ films

Yuanbin Xue[a], Cuihuan Geng[a], Xiaojing Bai[a], Huali Hao[b,*]

[a] Henan International Joint Laboratory of Nanocomposite Sensing Materials, Anyang Institute of Technology, Anyang, China, 455000

[b] School of Civil Engineering, Wuhan University, Hubei, China, 430072

[*] Corresponding author

*E-mail address:* haohuali@whu.edu.cn

### Introduction of quench molecular dynamics (QMD) approach

A QMD calculation combines molecular dynamics and geometry minimization (i.e. quench) in a single simulation. It performs a standard molecular dynamics calculation, but an additional structural optimization is also performed every ***n*** steps (***n*** is specified by the user). Effectively, molecular dynamics is used to sample many different configurations. By comparing the energies of these sampled structures, it is more likely to obtain the global minimum configuration, not just the local minimum one. So, QMD method provides a means of searching the configuration space for the lowest energy configuration.

In this study, a total of 10000 molecular dynamics steps were performed, and a quench, or geometry optimization, is performed every 500 steps. This means that 20 adsorption structures were sampled in each simulation, and the optimal adsorption configuration was determined by comparing the energies of these 20 structures.

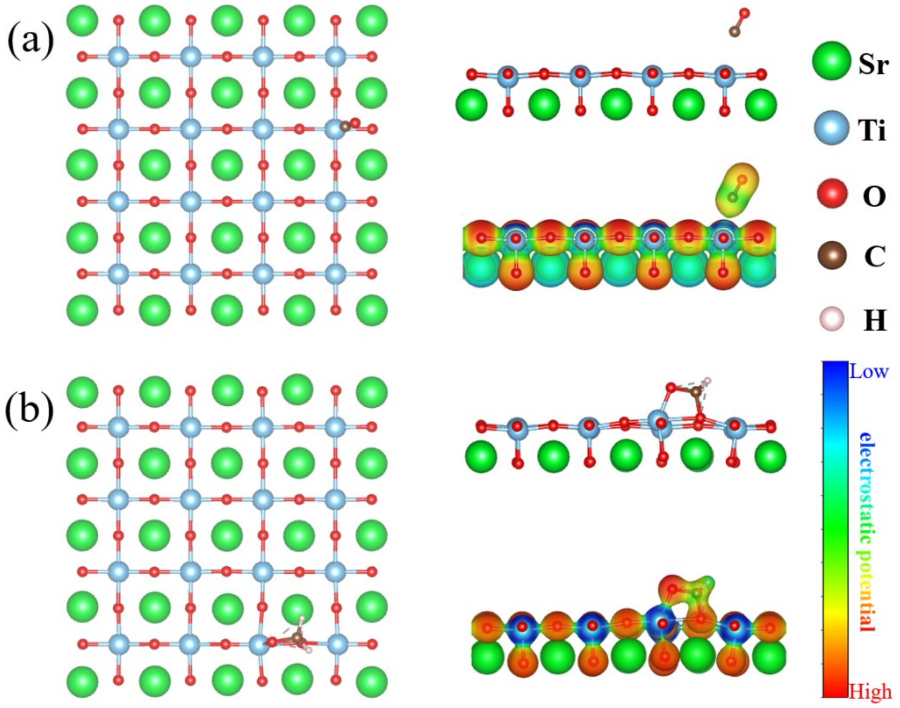

**Fig. S1.** The top view (left) and side view (top right) of the adsorption configurations of (a) CO and (b) $CH_2O$ on the pristine Ti-O surface of 2D STO film. On the bottom right of each figure is the side view of the electronic electrostatic potential mapped to electron density isosurface.

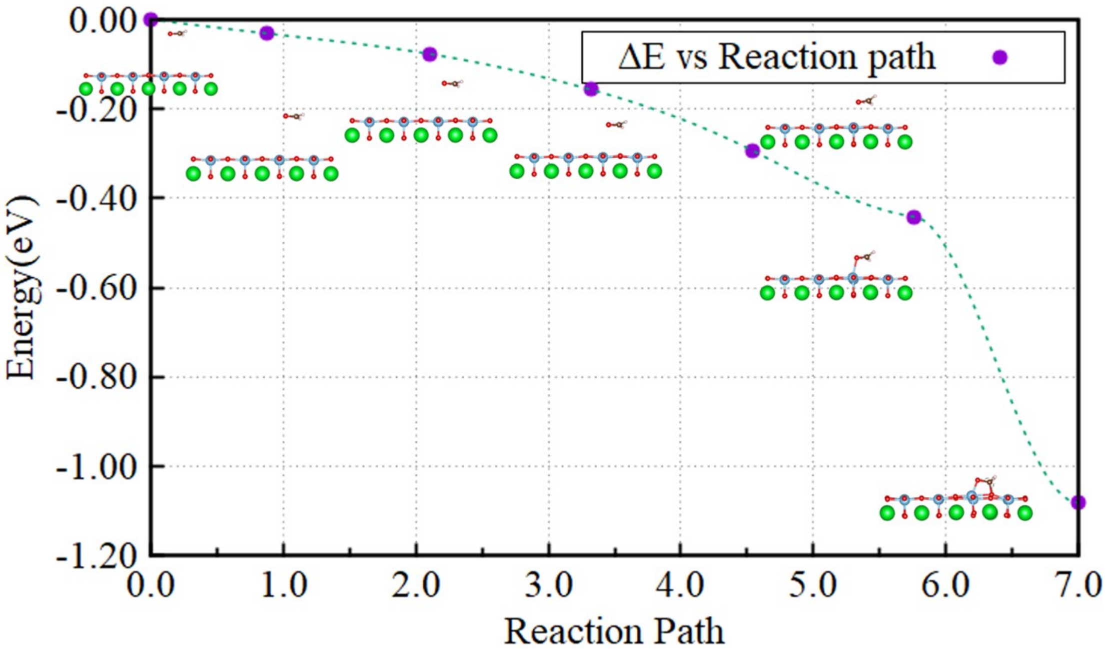

**Fig. S2.** Variation of relative energy ($\Delta E$) of the $CH_2O$ plus 2D STO film system along the adsorption path. The insets show the side view of the initial, intermediate, and final configurations of $CH_2O$ on the Ti-O surface.

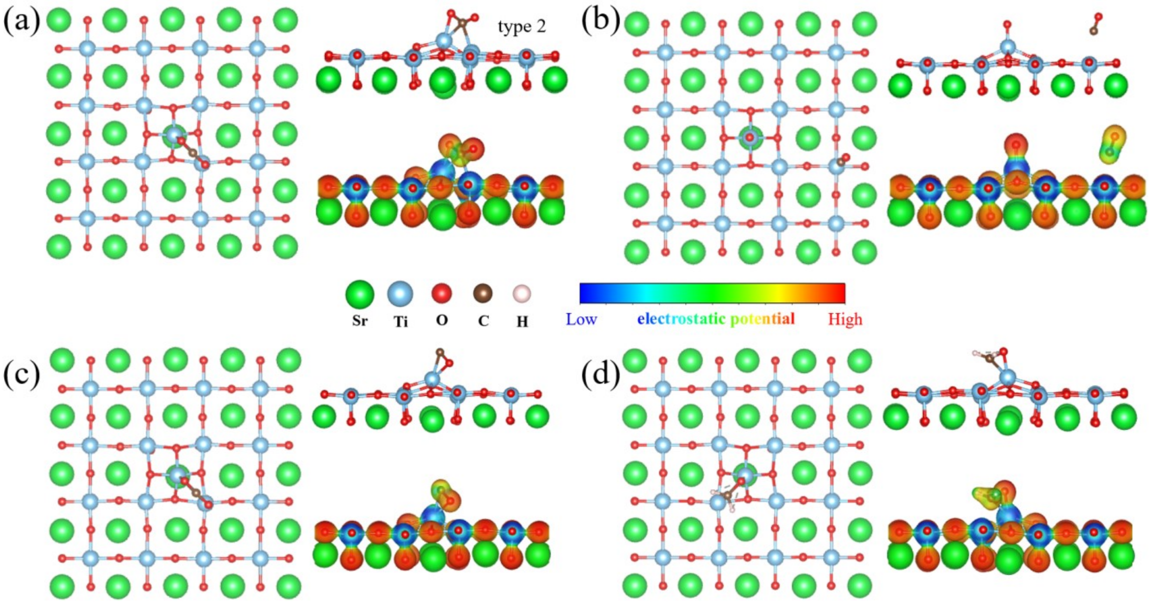

**Fig. S3.** The top view (left) and side view (top right) of the adsorption configurations of (a) $CO_2$ (type2), (b) dissociative $CO_2$, (c) CO and (d) $CH_2O$ at the Ti adatom site on the Ti-O surface of 2D STO film. On the bottom right of each figure is the side view of the electronic electrostatic potential mapped to electron density isosurface.

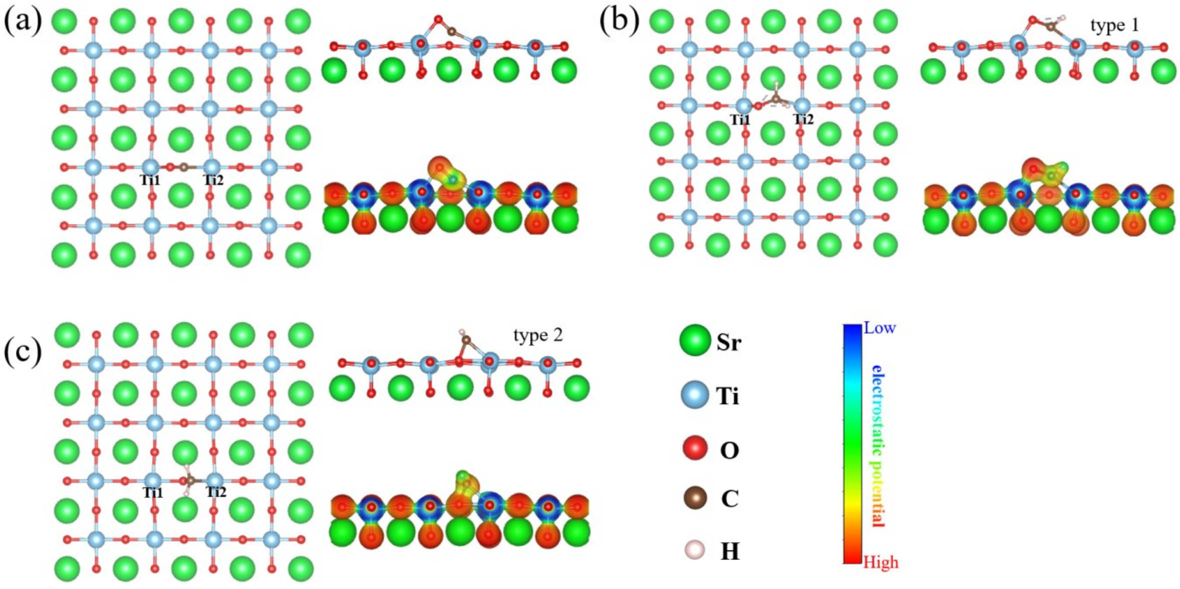

**Fig. S4.** The top view (left) and side view (top right) of the adsorption configurations of (a) CO, (b) $CH_2O$ (type 1), and (c) $CH_2O$ (type 2) at the O vacancy site on the Ti-O surface of 2D STO film. On the bottom right of each figure is the side view of the electronic electrostatic potential mapped to electron density isosurface.

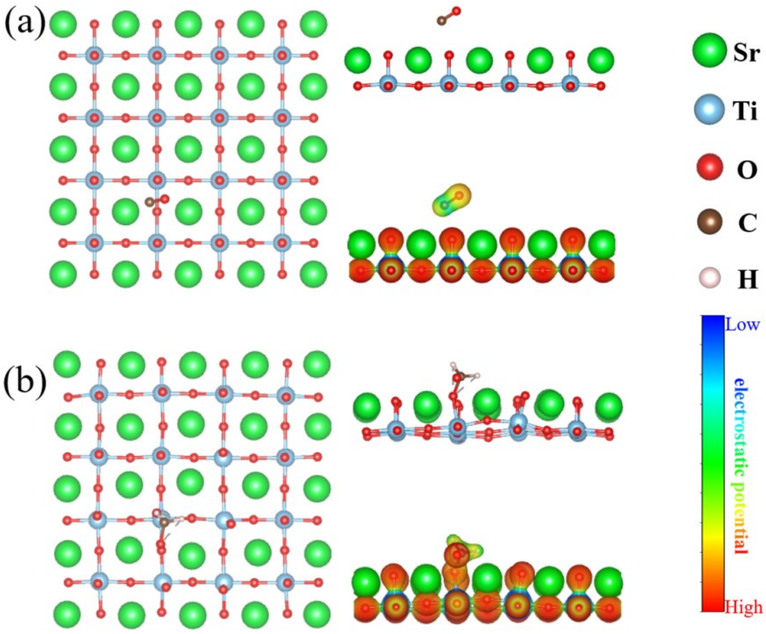

**Fig. S5.** The top view (left) and side view (top right) of the adsorption configurations of (a) CO and (b) $CH_2O$ on the pristine Sr-O surface of 2D STO film. On the bottom right of each figure is the side view of the electronic electrostatic potential mapped to electron density isosurface.

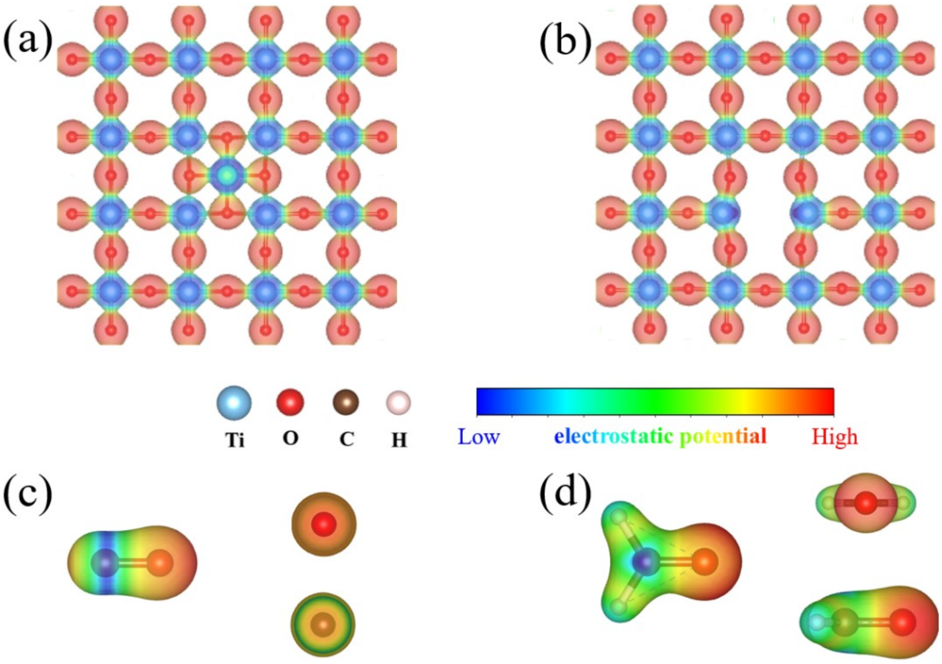

**Fig. S6.** Electronic electrostatic potential mapped electron density isosurface of (a) Ti adatom doped Ti-O surface, (b) O vacancy doped Ti-O surface, (c) CO molecule, and $CH_2O$ molecule. Colored isosurfaces from different perspectives are given in (c) and (d).

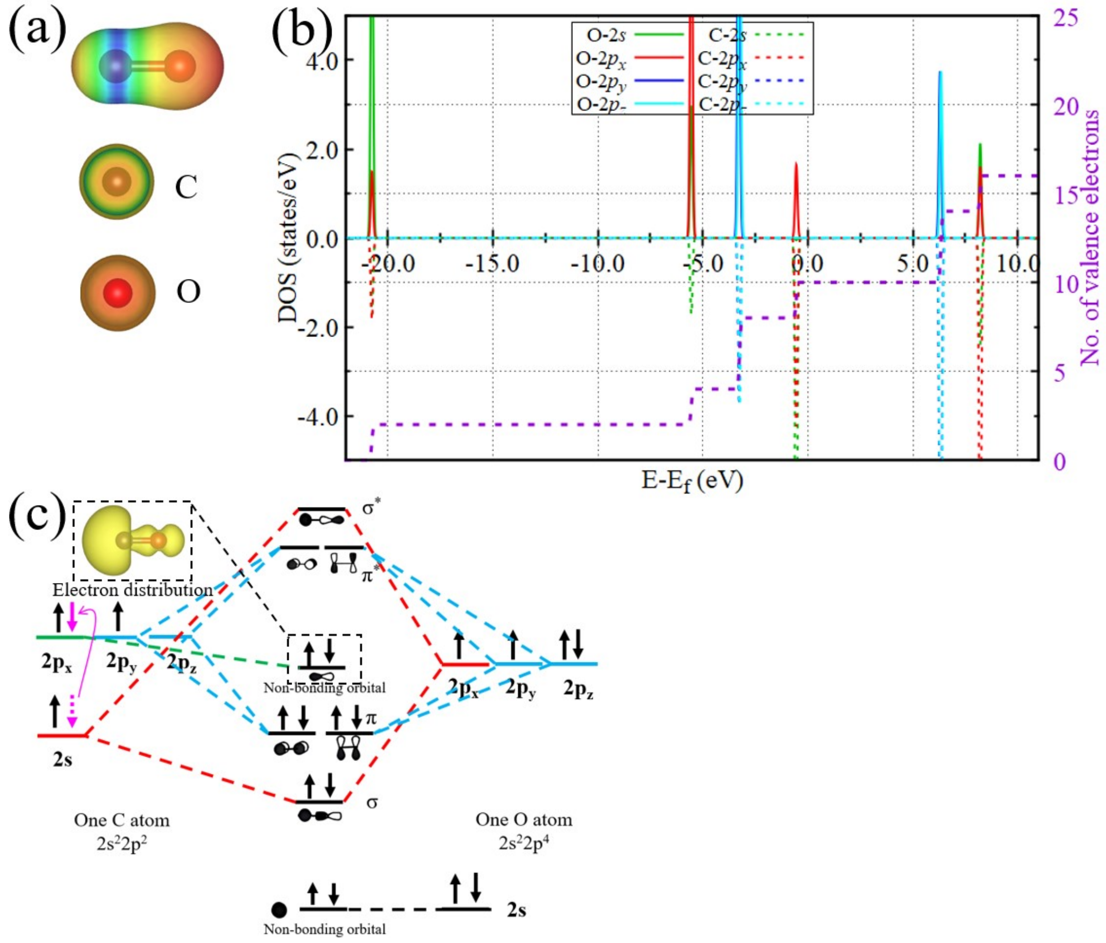

**Fig. S7.** (a) the electronic electrostatic potential mapped electron density isosurface, (b) the calculated DOS, and (c) the schematic energy level diagram of molecular orbitals for CO. The colored isosurfaces in (a) are given in different perspectives. The distribution of electrons in HOMO of CO is also shown in (c).

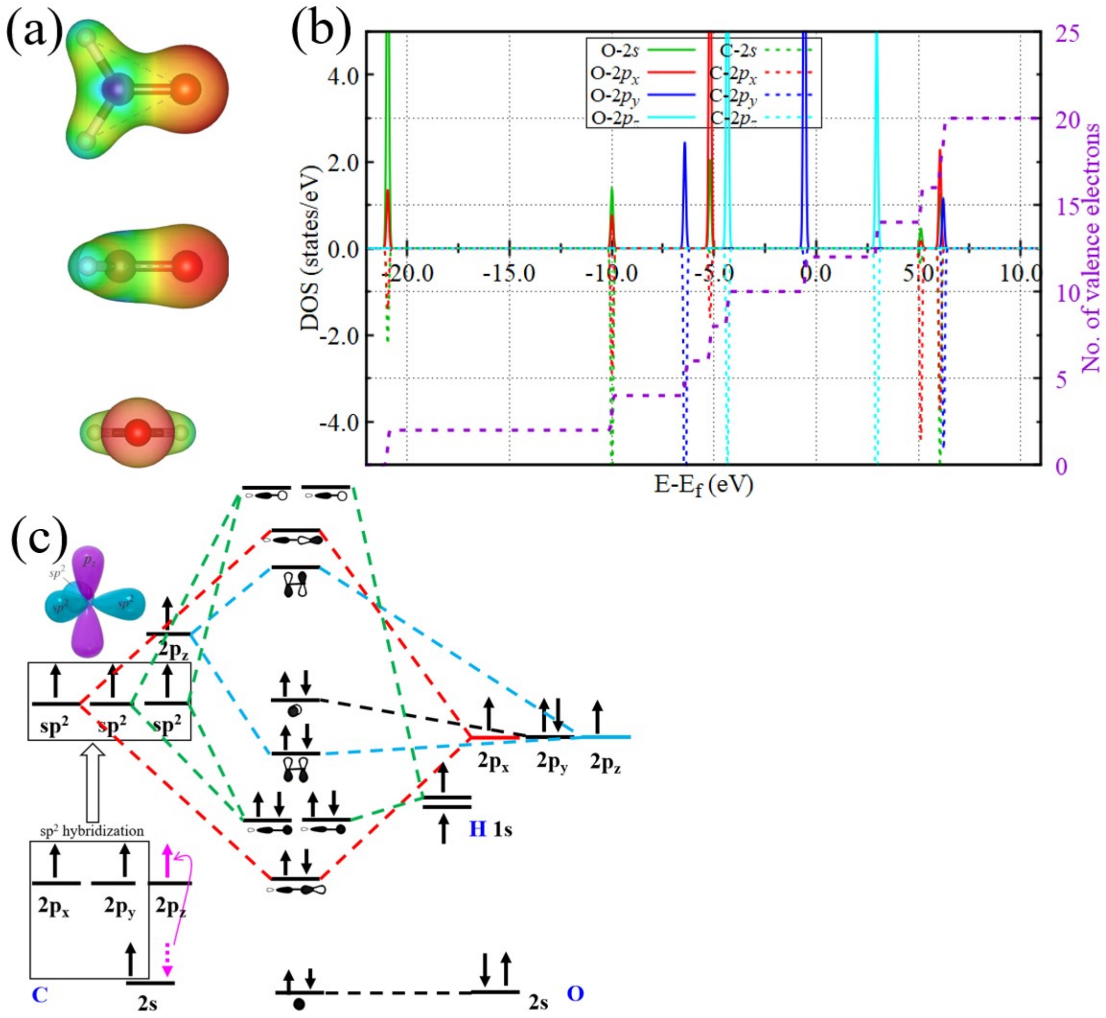

**Fig. S8.** (a) the electronic electrostatic potential mapped electron density isosurface, (b) the calculated DOS, and (c) the schematic energy level diagram of molecular orbitals for CH$_2$O. The configuration of the *sp*$^2$ hybridized orbitals of the C atom of CH$_2$O is also shown in (c).

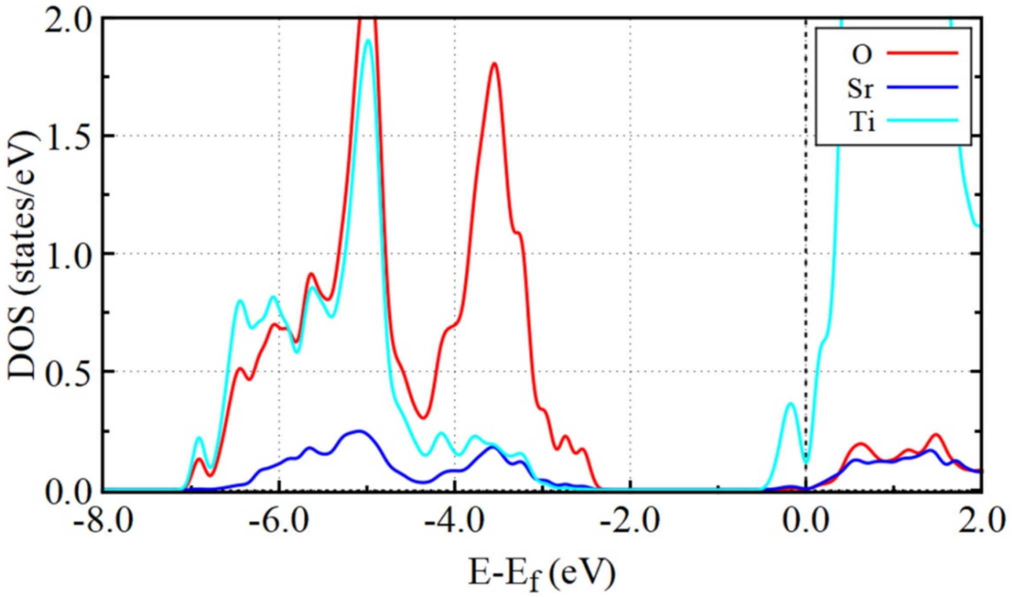

**Fig. S9.** The element-resolved DOS of O vacancy doped 2D STO film. The Fermi energy ($E_f$) is set as reference zero point.

**Table S1** The adsorption energy ($E_{ad}$) of M (M=CO and $CH_2O$) on pristine Ti-O surface (M@Ti-O), pristine Sr-O surface (M@Sr-O), Ti adatom (M@Ti) and O vacancy (M@Vo), respectively, and the average variation in C-O bond length ($\Delta l_{C\text{-}O}$), C-O bond ICOHP ($\Delta ICOHP_{C\text{-}O}$), electron transfer number for M ($\Delta n_{tot,}$), C atom ($\Delta n_C$), and O atom ($\Delta n_O$) after adsorption. The units of $E_{ad}$, $\Delta l_{C\text{-}O}$, $\Delta ICOHP_{C\text{-}O}$, and $\Delta n$ are eV, Å, eV and ***e***, respectively. ***e*** stands for a single electron, and the positive (negative) sign indicates an increase (decrease) in the number of valence electrons.

| Configuration | $E_{ad}$ | $\Delta l_{C\text{-}O}$ | $\Delta ICOHP_{C\text{-}O}$ | $\Delta n_{tot}$ | $\Delta n_C$ | $\Delta n_O$ |
|---|---|---|---|---|---|---|
| CO@Ti-O | -0.372 | ~0 | ~0 | ~0 | ~0 | ~0 |
| CO@Sr-O | -0.274 | ~0 | ~0 | ~0 | ~0 | ~0 |
| CO@Ti | -0.549 | 0.098 | 4.839 | +0.51 | +0.40 | +0.11 |
| CO@Vo | -1.458 | 0.088 | 5.291 | +0.75 | +0.65 | +0.10 |
| $CH_2O$@Ti-O | -1.082 | 0.166 | 6.200 | +0.22 | -0.11 | +0.12 |
| $CH_2O$@Sr-O | -1.098 | 0.165 | 4.942 | +0.69 | -0.12 | +0.43 |
| $CH_2O$@Ti | -2.887 | 0.216 | 6.578 | +0.72 | +0.49 | +0.07 |
| $CH_2O$@Vo (type1) | -2.067 | 0.190 | 6.678 | +0.85 | +0.45 | +0.09 |
| $CH_2O$@Vo (type2) | -2.957 | 0.230 | 7.457 | +0.93 | +0.41 | +0.37 |